Human Molecular Genetics, 2007, Vol. 16, No. 8 ***874–886***
doi:10.1093/hmg/ddm032
Advace Access publication on February 22, 2007

Multiple roles for neurofibromin in skeletal development and growth

Mateusz Kolanczyk[1,2], Nadine Kossler[1,2], Jirko Kühnisch[2], Liron Lavitas[1], Sigmar Stricker[1,2], Ulrich Wilkening[1,2], Inderchand Manjubala[3], Peter Fratzl[3], Ralf Spörle[4], Bernhard G. Herrmann[4], Luis F. Parada[5], Uwe Kornak[1,2] and Stefan Mundlos[1,2,*]

[1]FG Development and Disease, Max Planck Institute for Molecular Genetics, Berlin, Germany, [2]Institute for Medical Genetics, Charitè, Universitätsmedizin Berlin, Germany, [3]Max-Planck Institute of Colloids and Interfaces, Potsdam, Germany, [4]Department of Developmental Genetics, Max Planck Institute for Molecular Genetics and Institut für Medizinische Genetik, CBF, Charité, Berlin, Germany and [5]University of Texas Southwestern Medical Center, Dallas, TX 75390, USA

Received February 13, 2007; Revised and Accepted February 14, 2007

Neurofibromatosis type 1 (NF1) is a prevalent genetic disorder primarily characterized by the formation of neurofibromas, café-au-lait spots and freckling. Skeletal abnormalities such as short stature or bowing/pseudarthrosis of the tibia are relatively common. To investigate the role of the neurofibromin in skeletal development, we crossed Nf1flox mice with Prx1Cre mice to inactivate Nf1 in undifferentiated mesenchymal cells of the developing limbs. Similar to NF1 affected individuals, $Nf1^{Prx1}$ mice show bowing of the tibia and diminished growth. Tibial bowing is caused by decreased stability of the cortical bone due to a high degree of porosity, decreased stiffness and reduction in the mineral content as well as hyperosteoidosis. Accordingly, osteoblasts show an increase in proliferation and a decreased ability to differentiate and mineralize *in vitro*. The reduction in growth is due to lower proliferation rates and a differentiation defect of chondrocytes. Abnormal vascularization of skeletal tissues is likely to contribute to this pathology as it exerts a negative effect on cortical bone stability. Furthermore, Nf1 has an important role in the development of joints, as shown by fusion of the hip joints and other joint abnormalities, which are not observed in neurofibromatosis type I. Thus, neurofibromin has multiple essential roles in skeletal development and growth.

INTRODUCTION

Human conditions that predispose to cancer usually carry heterozygous germline (inherited) mutations in growth regulator genes that are essential for organized cell growth and differentiation. Affected individuals are at significant risk to develop benign or malignant tumors early in life because only one additional genetic alteration (loss of the wt allele) is needed to facilitate tumorigenesis. Cells that have lost both copies of the tumor suppressor gene have a growth advantage over wt cells. In a susceptible environment, this 'second hit' may result in tumor formation. Intriguingly, many cancer predisposition syndromes are associated with non-tumor abnormalities that usually occur in an irregular and mosaic manner, indicating that similar mechanisms may account for these changes. Here, the second hit occurs during early stages of development revealing important functions of the mutated gene during embryogenesis or fetal growth.

One example for such a condition is neurofibromatosis type 1 (NF1; OMIM #162200), a tumor predisposition syndrome mainly characterized by the occurrence of pigmented skin lesions (café-au-lait spots) and the formation of tumors (neurofibromas) along peripheral and optic nerves that are derived from nerve sheath (Schwann) cells (1). Although these changes are a relatively constant finding, a wide variety of non-tumor manifestations have been described that occur in association with NF1 at a lower frequency. These include hypertension, macrocephaly and a variety of skeletal changes such as scoliosis, vertebral dysplasia, short stature, sphenoid wing dysplasia and pseudarthrosis or bowing of the tibia (2,3). Other less common abnormalities of the skeleton include local overgrowth, abnormalities of the rib cage, genu

*To whom correspondence should be addresssed. Email: mundlos@molgen.mpg.de

varum/valgum, lytic bone lesions, osteosclerosis, rib fusion, absence of the patella, syndactyly and other congenital bone malformations (4). These clinical findings suggest a role for NF1 in skeletal development and have raised the question whether skeletal dysplasia is a primary feature of NF1 (2). Investigations of affected skeletal tissue in tibial pseudarthrosis have shown additional mutations of the second NF1 allele indicating that the homozygous loss of NF1 function can be detrimental for normal bone development (5). Thus, like in NF1-mediated tumorigenicity, a loss of both NF1 alleles is likely to be required to cause the phenotype.

The molecular pathogenesis of NF1 has been elucidated by the identification of causative mutations in the gene which encodes neurofibromin. Neurofibromin is a large cytoplasmic protein with a small central region that shows homologies to the GTPase activating family of proteins (GAP), and therefore is termed the GAP-related domain (GRD) (6). Members of the Ras-GAP family share a similar function by negatively regulating a key signal transduction protein called p21-Ras. P21-Ras is a small G-protein involved in transmitting signals from various growth factor receptors to a large number of downstream signaling molecules that eventually alter gene expression in the nucleus (7). Thus, loss of neurofibromin activity is expected to lead to the inability to shut off activated p21-Ras with subsequent aberrant growth promoting signals. This is similar to mutant forms of RAS found in human tumors that have greatly decreased GTPase activity, resulting in accumulation of RAS in the GTP-bound active form.

Dysregulation of Ras proteins by activating mutations, overexpression or upstream activation is a common and extensively studied phenomenon in human tumors. In contrast, much less is known about the physiological role of Ras in development and tissue maintenance. One route of Ras activation is through fibroblast growth factor (FGF) signaling. FGFs are secreted molecules, which function through the activation of specific tyrosine kinase receptors, the FGF receptors (FGFR), which transduce the signal by activating a variety of pathways including the Ras/MAP kinase pathway. In the growth plate, FGFR3 serves as a negative regulator of chondrocyte proliferation and differentiation and activating mutations result in skeletal disease and short stature (8). Interestingly, mutations in PTPN11, a gene encoding the nonreceptor protein tyrosine phosphatase SHP2 involved in the transduction of FGFR signaling to Ras, result in Noonan (OMIM #163950) syndrome, a condition also characterized by short stature (9). A phenocopy of this condition can be caused by mutations in NF1 (neurofibromatosis–Noonan syndrome, OMIM #601321) and by *de novo* germline mutations of the KRAS gene (10).

The role of Nf1 in tumor formation and development has been studied in mice with inactivated Nf1 alleles (11–13). Affected mice exhibit neural closure defects (exencephaly) and cardiovascular abnormalities including structural malformations of the outflow tract of the heart and enlarged endocardial cushions. These Nf1-deficient embryos die between embryonic days 12.5 and 13.5, presumably due to the cardiac vessel defect. In contrast, inactivation of NF1 in the neural crest does not cause cardiac defects but results in tumors of neural crest origin resembling those seen in humans with NF1 (11). To investigate the function of NF1 in skeletal development, we inactivated Nf1 during early mouse limb development using the transgenic mouse line Prx1Cre. In these mice Cre is expressed in undifferentiated mesenchymal cells in the limb bud resulting in efficient inactivation of the Nf1 gene in the appendicular skeleton (14). This approach is likely to reflect the situation in NF1 patients with irregular, non-generalized lesions. Such lesions can be expected to be due to mutational events that inactivate the remaining wt NF1 allele during early stages of development resulting in NF1 inactivation in entire cell lineages. Our results indicate that Nf1 has multiple roles in skeletal development including joint formation, growth plate function, osteoblast differentiation, and control of vessel growth. Thus, short stature and bowing of the tibia, skeletal defects frequently associated with NF1, are caused by a primary function of neurofibromin in skeletal development and homeostasis.

RESULTS

Because Nf1 inactivation results in early lethality due to a severe heart malformation, we used a conditional inactivation approach to ablate Nf1 function specifically in the limb skeleton. Mice with a conditional allele of Nf1 ($Nf1^{flox}$) susceptible to Cre-mediated recombination *in vivo* were crossed with Prx1Cre transgenic mice ($Prx1^{cre}$). Cre recombinase in $Prx1^{cre}$ mice is expressed in early and late stages of limb bud development, in the lateral plate mesoderm and the cranial part of the developing head mesenchyme (14) (Supplementary Material, Fig. S1A). We used an allele-specific PCR to determine the Cre recombinase-mediated excision rate in osteoblasts, chondrocytes, bone marrow derived endothelial cells and osteoclasts (Fig. 1A). As expected, only osteoclasts, which are of hematopoietic descent, showed no recombination, whereas all other cell types underwent efficient Cre-mediated excision of the $Nf1^{flox}$ allele.

Nf1 is essential for the development of joints

$Nf1^{flox/+};Prx1^{cre} \times Nf1^{flox/flox}$ crossings gave the expected Mendelian ratios of $Nf1^{flox/flox};Prx1^{cre}$ mice, which we abbreviate as $Nf1^{Prx1}$ in the following. Newborn $Nf1^{Prx1}$ mice were easily recognized at birth due to their inability to bend their hind limbs at the hip joint (Fig. 1B). Examination of the stained skeletons and histological analysis revealed cartilaginous fusions of the hip joints (Fig. 1C). We observed abnormal hips in all animals but the phenotype varied between complete and partial fusion. Analysis of the hip joint at the age of 4 weeks using μCT demonstrated a distorted morphology of the femoral neck and the femoral head (Fig. 1D). We investigated other joints for anomalies to see if this phenomenon was restricted to the hip. The shoulder joint appeared normal, but the elbow joint was severely deformed (data not shown). Although knee joints of $Nf1^{Prx1}$ animals were not fused, serial sections of stage P14 revealed several abnormalities (Fig. 1E). Most important was a drastic reduction of the size of the menisci, which also points to a defect in joint cavitation.

To determine the normal time point of joint development in the hip, we investigated wt animals at stages E12.5–E15.5 by

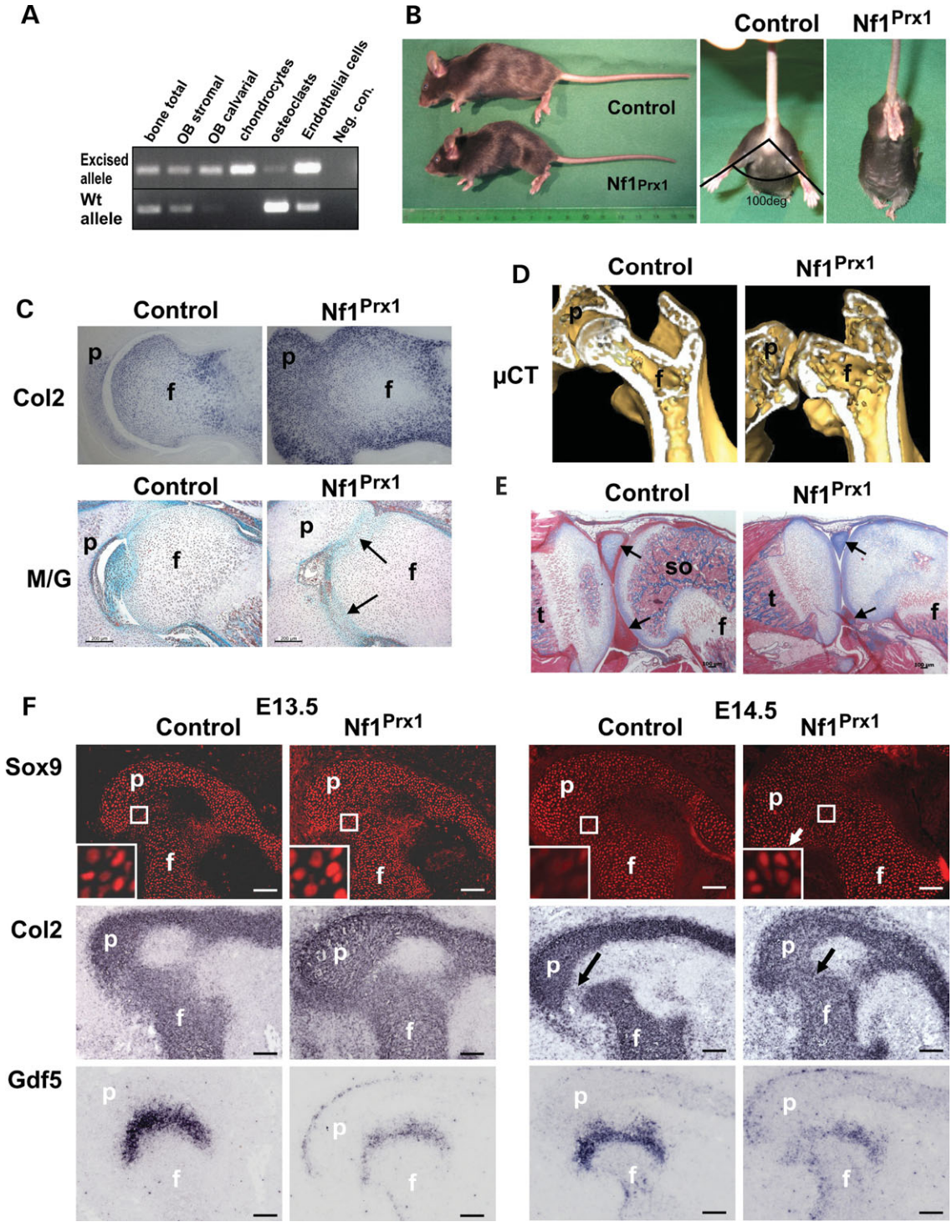

Figure 1. Nf1 is involved in the development of joints. (**A**) Prx1-Cre mediated recombination in osteoblasts (OB), endothelial cells (CD31 positive cells derived from long bones) and in chondrocytes, but not in osteoclasts. 'Bone total' refers to cells isolated from the long bone shaft before culturing, 'OB stromal' to stromal osteoblasts differentiated from this cell suspension and 'OB calvarial' to osteoblasts derived from cranial bones. (**B**) $Nf1^{Prx1}$ mice have short limbs and exhibit an impaired hip joint movement, due to a cartilaginous fusion of the femur head with the pelvis. (**C**) *In situ* hybridization for Col2a1 and Masson/Goldner staining showing hip joint fusion at P1 and P4, respectively. Arrows identify the cartilaginous fusion of pelvis and femur head at P4. (**D**) μCT of proximal femur showing severe malformation of the hip joint at P42. (**E**) Sagittal section through knee joint. $Nf1^{Prx1}$ mice have small menisci (arrow) and a delay of secondary ossification (so). (**F**) Analysis of hip joint development at E13.5 (left panel) and E14.5 (right panel) showing immunohistochemical staining for Sox9, *in situ* hybridization for Col2a1 and Gdf5, from top to bottom. Note nuclear localization of Sox9 protein in the entire cartilage anlage of pelvis (p) and femur (f). At E14.5, control animals develop a joint interzone where Sox9 shows cytoplasmic localization, and Col2a1 expression is downregulated. In the corresponding region, $Nf1^{Prx1}$ mice show persistence of Sox9 nuclear localization and Col2a1 expression (arrow). Gdf5 is expressed in the future joint region but is downregulated in $Nf1^{Prx1}$ mice at E13.5 and E14.5. t, tibia; f, femur; p, pelvis. Scale bars: 100 μm.

performing serial transverse sections through the area of the femur/pelvis anlage (Fig. 1F). A small cartilaginous condensation present at E12.5 (data not shown) developed into cartilaginous anlage of the future pelvis and the adjacent femur at E13.5. Similar to other future joint regions, femur and pelvis are fused as one cartilaginous anlage at this stage, as indicated by a continuous expression pattern of Col2a1. Expression of Gdf5 was observed at the site of the future joint at E13.5, but expression levels were clearly lower in mutant mice indicating that the process of joint cavity formation was not initiated. In controls a joint interzone became apparent and the femur and pelvis anlage began to separate at E14.5, whereas this process was severely disturbed in $Nf1^{Prx1}$ mice. Sox9 is an essential regulator of chondrocyte cell fate decision (15). In control joints, we observed a normal nuclear distribution of Sox9 throughout the cartilage anlage at E13.5. Concomitant with the formation of an interzone at E14.5, cells of this region showed a shift of Sox9 localization from the nucleus to the cytoplasm. In contrast, the nuclear localization persisted in all cells of the cartilage anlage in $Nf1f^{Prx1}$ mice (Fig. 1F upper panel). Thus, the hip joint phenotype observed in the $Nf1f^{Prx1}$ mutant animals is due to a lack of joint cavity initiation caused by an impaired chondrocyte de-differentiation in the presumptive joint region.

Loss of Nf1 recapitulates human Nf1-associated tibial bowing

Congenital pseudarthrosis of the tibia is a rare but severe complication of NF1. It is characterized by recurrent fractures of the lower leg in early childhood. Callus formation fails and bone healing tends to be insufficient. The first sign of this skeletal complication is anterolateral bowing of the tibia. Using optical projection tomography (OPT) to construct a three-dimensional image of the hind limbs, we observed an anterolateral bowing of the tibia in all $Nf1^{Prx1}$ mutants (Fig. 2A, Supplementary Material, Movies) and compared it with the bowing in human NF1 cases (for comparison, see Fig. 2B). The bowing started before birth, as it was already apparent in newborns. It progressed thereafter but did not worsen after 2 weeks of age. The fibula was relatively mildly affected with slight bowing in the distal part detectable at P7. The phenotype is fully penetrant, as among 185 pups born in 25 litters, we observed 62 mutant animals, all of which exhibited conspicuous tibia bowing. Because bowing may occur due to a reduced stiffness, we investigated the physical properties of cortical bone in $Nf1^{Prx1}$ mutants. We performed back-scattered electron (BSE) imaging of cortical bone from 2-week-old mice (for description see Materials and Methods). In normal bone, the porosity is at the order of 10% ($\pm$7% SD) mostly due to irregularly distributed osteocyte lacunae (16). In $Nf1^{Prx}$ mutants we observed an increased porosity (24% $\pm$9% SD), which was not correlated to osteocyte lacunae (Fig. 2D). Pore sizes were up to 50 μm, whereas osteocyte lacunae are just a few microns (Fig. 2C, left panel). Using the same technique, we found a significant ($P < 0.001$) decrease in tissue calcium content in mutants (Fig. 2D). To determine the micrometer level elastic and plastic response of the cortical bone, we used the nanoindentation device, by making small indents (<1 μm) on polished plastic-embedded cortical bone. The nanoindentation modulus in bone samples was found to be decreased significantly from 13–16 GPa in controls to 9–11 GPa in mutant samples (Fig. 2E). Note that nanoindentation measures the material (matrix-mineral composite) response very locally (at a scale much smaller than the pores and within bone matrix only) and is not influenced by the porosity.

To investigate the possible mechanisms underlying the observed cortical porosity, we performed serial sections of the diaphysis of the tibia. The cortical bone of mutants showed abnormally large non-mineralized areas populated by blood vessels and fibroblast-like cells. CD34 staining confirmed that, in contrast to controls, the non-mineralized areas in $Nf1^{Prx1}$ bones were rich in blood vessels penetrating the cortex from the periosteum to the bone marrow cavity (Fig. 2F). We did not observe an increase in osteoclast number within the porosities (data not shown). Histological analysis of the appendicular bone showed an increased thickness of the osteoid (Fig. 2G) and an increased number of osteoblasts, indicating abnormalities in osteoblast differentiation and/or proliferation in $Nf1^{Prx1}$ mice.

Altered osteoblast differentiation and proliferation by loss of Nf1

To identify the reason for the reduction of bone strength and mineralization, we investigated osteoblast differentiation *in vitro*. For this purpose, we used calvarial osteoblasts obtained from wt and mutant P5 animals, as cultivation of calvarial osteoblasts is a well-established method to study *in vitro* bone formation, and Prx1 is known to be expressed in the developing skull vault (14). Nf1 excision rate analysis showed that the Prx1-driven Cre-recombinase had efficiently excised the floxed allele in these cells (Fig. 1B). Alkaline phosphatase (ALP) activity was significantly reduced in $Nf1^{Prx1}$ osteoblasts after osteogenic stimulation (Fig. 2H). In addition, mineralization, a hallmark of osteoblast differentiation, was diminished (Fig. 2I). These findings were mirrored by reduced alkaline phosphatase (Akp2) mRNA levels and by a decrease of the terminally differentiated osteoblast markers integrin-binding sialoprotein (Ibsp) and osteocalcin (Ocn), which are normally expressed at this stage. In contrast, the early differentiation marker osteopontin (Opn) appeared to be strongly induced (Fig. 2J). Thus, a loss of Nf1 in mesenchymal progenitor cells or immature osteoblasts leads to an accumulation of incompletely differentiated osteoblasts *in vitro* and *in vivo*. To test a possible effect on proliferation, the osteoblast cell division rate was quantified by BrdU labeling (Fig. 2K). The labeling index of mutant cells was increased when compared with controls. Thus, loss of Nf1 results in increased osteoblast proliferation, similar to the effect observed in other cell types after Nf1 inactivation.

Inactivation of Nf1 results in growth retardation and abnormal growth plates

$Nf1^{Prx1}$ mice exhibit congenital limb shortening (Fig. 3A and B). Measurements of bone growth over time demonstrated a 25% reduction in size of all long bones by P7 in the mutant animals (Supplementary Material, Table S1). This growth defect correlated with an abnormal growth plate with

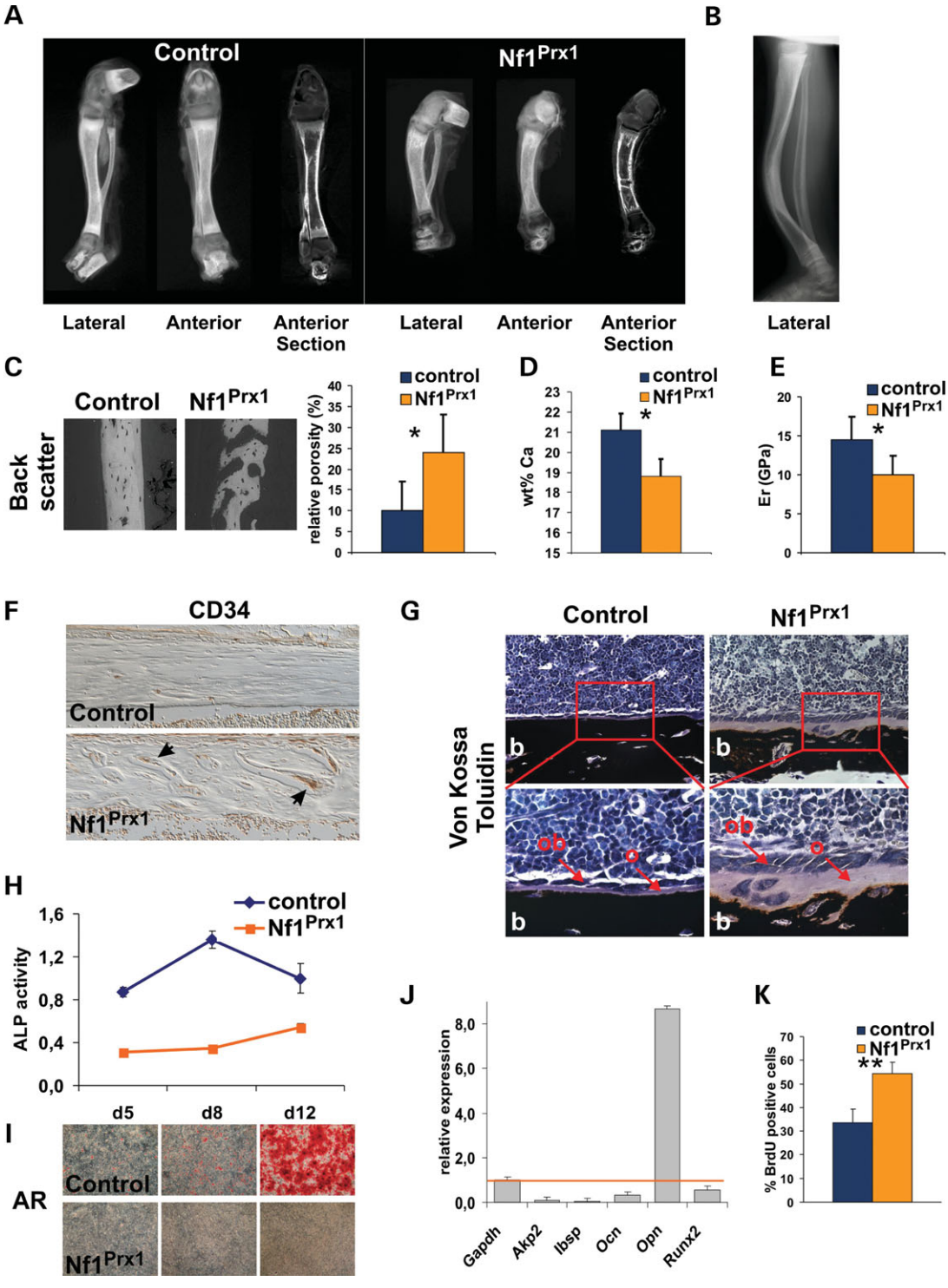

Figure 2. Loss of Nf1 recapitulates the human NF1-associated bone phenotype. (**A**) OPT performed on Alizarin/Alcian blue stained tibia at stage P7 with optical cross-section shown on the right. Note bowing of tibia in $Nf1^{Prx1}$ animals. (**B**) Bowing of tibia in an NF1 patient. (**C**) BSE images showing increased porosity in $Nf1^{Prx1}$ cortical bone of the tibia at P14. (**D**) Reduction in $Nf1^{Prx1}$ cortical bone calcium content as revealed by the analysis of BSE images. Quantification of the relative porosity is shown on the right. (**E**) A reduced elastic modulus Er(GPa) in transverse sections of mutant cortical bone when compared with controls at P14 determined using nanoindentation—see Materials and Methods for more information. (**F**) CD34-immunostained vessels within porosities of P14 tibia cortex of mutant but not control bone (arrows). (**G**) Thickening of osteoid and thinning of cortical bone (b) as well as increased number of osteoblasts in the femur of P14 $Nf1^{Prx1}$ mice (arrows). (**H**) $Nf1^{Prx1}$ calvarial osteoblasts exhibit decreased ALP activity and (**I**) reduced mineralization of extracellular matrix stained by alizarin red (AR) during *in vitro* differentiation. (**J**) Expression of osteoblast differentiation marker genes on the eighth day of primary calvarial osteoblasts differentiation measured by quantitative PCR. Mutant cells show increased expression of Osteopontin (Opn) and downregulation of alkaline phosphatase (Akp2), integrin binding sialo protein (Ibsp), osteocalcin (Ocn) and Runx2 compared with controls. (**K**) Increased proliferation of mutant primary calvaria osteoblast compared to controls revealed by BrdU labeling.

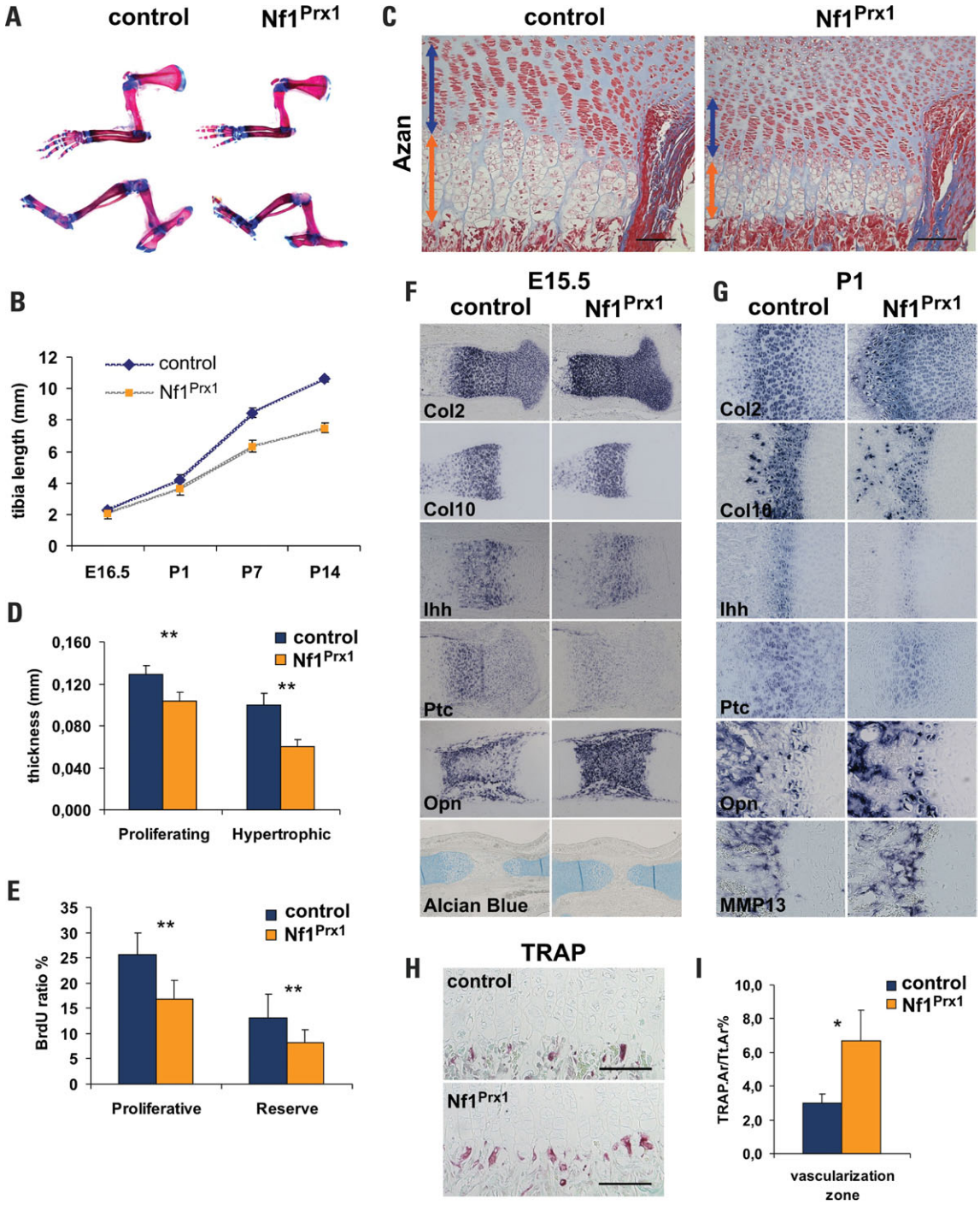

Figure 3. Inactivation of Nf1 results in growth retardation and abnormal growth plates. (**A**) Alizarin red/Alcian blue stained skeletons at P7. All elements of the appendicular skeleton are shorter in $Nf1^{Prx1}$ mice and exhibit slower growth (**B**) (see also Suplementary Material, Table S1). (**C**) Histology of the growth plate (proximal tibia) shows smaller proliferative (blue arrow) and hypertrophic zones (orange arrow). (**D**) Proliferative and hypertrophic zone thickness reduction measured morphometricaly in the femur of P14 $Nf1^{Prx1}$ mice. (**E**) BrdU labeling demonstrates a reduction of proliferation rate in both proliferative and reserve zone chondrocytes. (**F**) *In situ* hybridization of control and $Nf1^{Prx1}$ mice growth plates at E15.5 and in (**G**) newborns. Note reduced expression of Col10a1, Ihh and Ptc and increased expression of Opn and MMP13. (**H**) TRAP staining and its (**I**) quantification show increased osteoclast number in the chondro-osseous junction of the P14 animals. Scale bars in (C and H): 100 μm.

narrowed hypertrophic and proliferative zones (Fig. 3C). Histomorphometric measurement of tibial growth plates showed significant reduction of the hypertrophic and proliferative zones (Fig. 3D). Moreover, the development of secondary ossification centers was clearly delayed (Fig. 1E). To determine whether reduced proliferation contributes to the shortening of long bones, we measured chondrocyte proliferation rates in control and mutant growth plates after BrdU labeling.

We found a reduction of the proliferation rate in mutant animals (Fig. 3E).

Marker gene expression in the different zones of the growth plate was evaluated by *in situ* hybridization at E15.5 and in newborn animals (P1) (Fig. 3F and G). We found no major difference in the expression of collagen type II (Col2a1), the major collagen of cartilage. Indian hedgehog (Ihh) is a major regulator of chondrocyte proliferation and differentiation. At both stages, Ihh expression was significantly reduced, a finding which was further corroborated by a decreased expression of patched (ptc), the Ihh receptor, which is a downstream target of Ihh. At P1, we found a reduced expression zone of Col10a1 corresponding to a reduced size of the hypertrophic zone. Osteopontin (Opn), which is expressed in the most terminal hypertrophic chondrocytes and in osteoblasts, was clearly upregulated at all stages investigated. This was paralleled by an increased expression of Mmp13, a metalloproteinase that acts synergistically with osteoclast-expressed Mmp9 to degrade the hypertrophic cartilage matrix. Histomorphometric quantification of the number of osteoclasts at the chondro-osseous junction revealed an increase in the number as well as the surface area of tartrate-resistant acidic phosphatase (TRAP)-stained cells indicating increased osteoclast activity (Fig. 3H,I).

To confirm the *in situ* hybridization results, we performed quantitative PCR of knee growth plates (Fig. 4A). We found a strong upregulation of Opn. Expression of Lef1 and Pea1, two transcription factors known to activate Opn, was also increased. Furthermore, we detected an upregulation of Sox9 and Mmp9. No significant regulation was found for different isoforms of VEGF, as well as for Runx2 and RANKL. Ihh, PTHrP and Col10a1 were downregulated. Western blots confirmed the upregulation of Sox9 and Opn (Fig. 4B). To further investigate the intrisic role of Nf1 in cartilage, we isolated chondrocytes from wt and $Nf1^{Prx1}$ growth plates to propagate them *in vitro*. After serum starvation, we were able to demonstrate increased level of GTP-Ras and pErk1/2 in mutant cells, whereas expression of Erk1 and Erk2 was not changed (Fig. 4C and D). p21/Waf1, an important regulator of cell proliferation was upregulated in $Nf1^{Prx1}$ cells.

Loss of Nf1 induces invasive blood vessel growth

In endochondral ossification, the formation of vessels is tightly coupled with osteoclast activity and both processes seem to be dependent on signals released from the growth plate through the activity of MMPs. The number and size of CD34-positive blood vessels invading the growth plate was significantly increased in $Nf1^{Prx1}$ mutant animals (Fig. 5A). Cartilage is one of the few tissues without significant vasculature. Nevertheless, proper vascularization adjacent to the growth plate is essential for bone growth. The groove of Ranvier is a circumferential indentation at the periphery of the growth plate containing a vascular plexus and osteoblast and chondrocyte progenitor cells (17). Compared with wt, the vessels in this structure were larger in $Nf1^{Prx1}$ mice and appeared unorganized (Fig. 5B). Furthermore, the vessels originating from the groove of Ranvier penetrated the growth plate between the proliferating and hypertrophic chondrocyte layer (Fig. 5C). Hence, not only the cortical bone but also the growth plate cartilage shows signs of abnormal vascularization which is likely to contribute to the complex skeletal phenotype.

DISCUSSION

This study shows that Nf1 is a major regulator of development and growth of the skeleton. The inactivation of Nf1 in mouse limbs recapitulates the human NF1-associated skeletal phenotypes in several aspects. Similar to NF1 affected individuals, $Nf1^{Prx1}$ mice show diminished growth, and, as a more specific sign, bowing of the tibia. These multiple effects on the skeleton are due to abnormal differentiation and proliferation of osteoblasts and growth plate chondrocytes, as well as an abnormal formation of vessels within the skeleton. Furthermore, we observed a defect in the development of joints, a phenotype which has so far not been described in NF1 patients. Our results support the hypothesis that osseous dysplasia is a primary feature of NF1 (2).

Nf1 is involved in the early steps of joint formation

During development, the vertebrate appendicular skeleton cartilaginous anlagen of the future bones are initially laid down as continuous elements without joints. In a later, highly coordinated process, joints are placed within the anlagen, thus creating the individual skeletal elements. This process involves, in principle, four steps: patterning, formation of an interzone with concomitant loss of the chondrocyte phenotype at the future joint, cavitation, a process which eventually gives rise to the joint space, and the development of a joint capsule (18).

As shown by the early fusions in the hip, Nf1 is important for joint patterning and the initial phase of joint formation, i.e. the formation of an interzone and the subsequent downregulation of genes characteristic for chondrocytes such as Col2a1 and Sox9. Several genes and pathways have been implicated in this process. Gdf5 is a signaling molecule of the BMP family which plays a pivotal role in joint formation, as shown by human and mouse Gdf5 mutants. Alterations of Gdf5 activity, either by activating mutations or by loss-of-function mutations of its inhibitor noggin result in joint fusions in humans (19). In the mouse, loss of Gdf5 results in smaller cartilaginous anlagen of the digits and a lack of joint formation (20). We observed a strong downregulation of Gdf5 expression in mutant hip joints, a finding which correlates well with the diminished interzone formation. Associated with the downregulation of Gdf5, we observed a persistence of nuclear Sox9 expression, a transcription factor essential for chondrocyte differentiation and one of the main regulators of collagen type II (Col2a1), the predominant collagen of cartilage (21). During interzone formation, Sox9 is no longer detectable in the nucleus of wt interzone cells, a shift in expression, which is likely to be important for interzone formation. With persistent nuclear expression of Sox9, cells in the presumptive interzone can be expected to remain chondrocytic, thus contributing to the joint fusion. Other pathways are likely to be involved in addition. Overexpression of an activated form of the FGFR1 in the cartilage results in joint fusions (22) indicating that activation of FGF-signaling

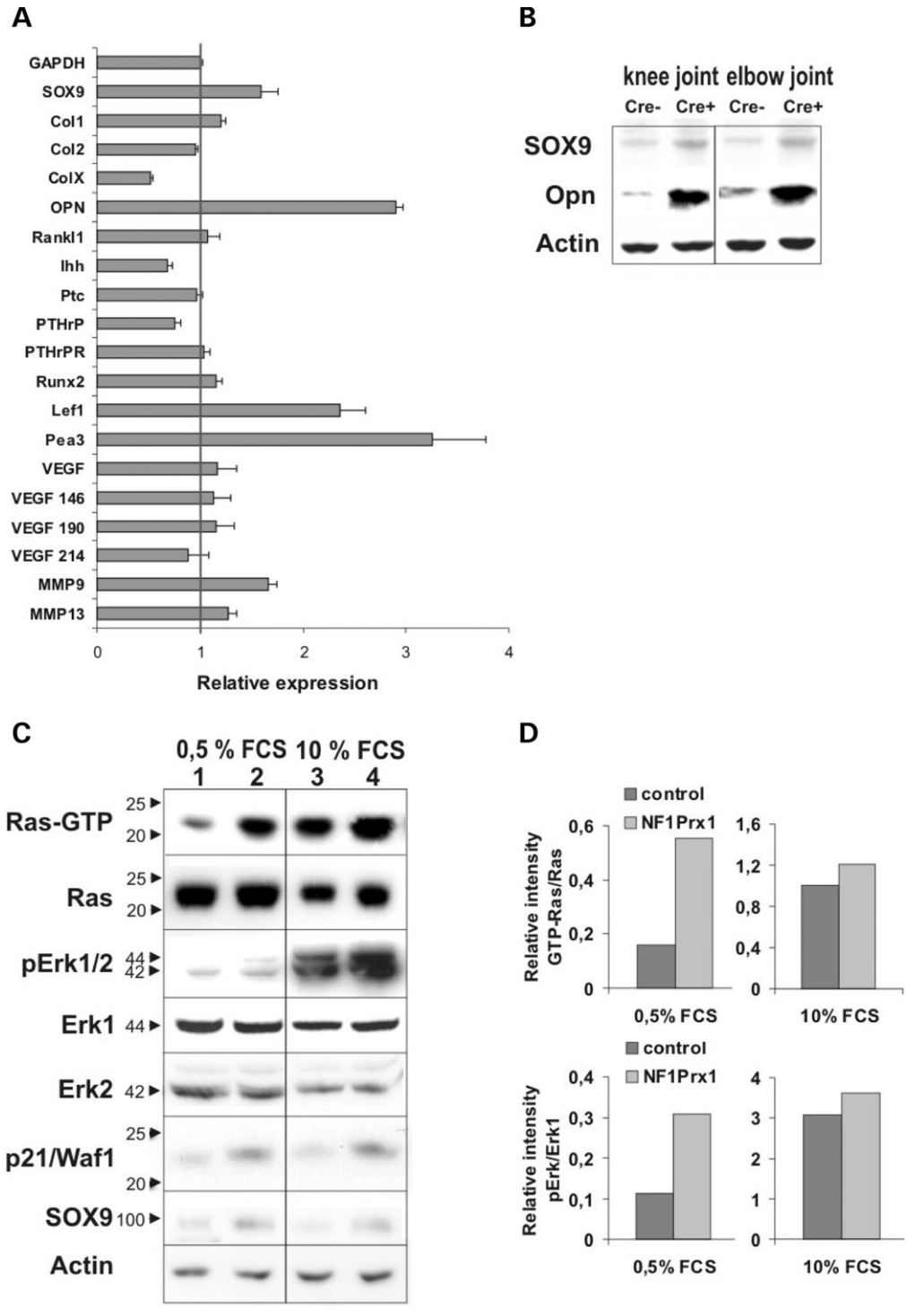

Figure 4. Deregulation of MAPK pathway, gene expression in primary chondrocytes and in epiphyseal cartilage. (**A**) Upregulation of Sox9, Opn, Lef1, Pea3 and Mmp9 and downregulation of Col10, Ihh and PTHrP expression in primary chondrocytes measured by quantitative PCR. (**B**) Western blot showing increased amounts of Sox9 and Opn protein in $Nf1^{Prx1}$ epiphyseal cartilage. (**C**) Western blots of primary chondrocyte whole cell lysates. Ras pathway status was determined under low serum condition (lanes 1–2). In a positive control experiment, Ras pathway was stimulated through 10 min treatment with 10% serum-containing media (lanes 3–4). Increased GTP-Ras and pERK1/2 levels were detected in $Nf1^{Prx1}$ cells (lanes 2 and 4) when compared with controls (lanes 1and 3); however, upon stimulation with 10% FCS (lanes 4 and 3), Ras activation becomes close to maximal and therefore difference between wt and mutant cells is less prominent. Mutant cells also exhibit increased levels of p21/waf1 and Sox9 expression. Positions of molecular weight markers were assigned at the left site of the panel. (**D**) Increased GTP-Ras/Ras and pErk/Erk1 ratios illustrating Ras pathway activation in $Nf1^{Prx1}$ cells as determined by densitometric analysis of western blots.

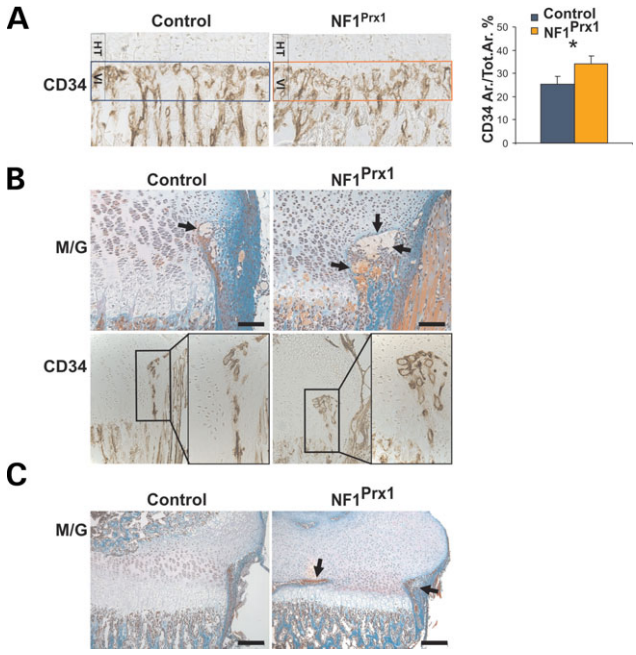

Figure 5. Altered vessel formation in $Nf1^{Prx1}$ mice. (**A**) Enhanced vascularization of the proximal tibia chondro-osseous junction in mutant mice revealed by CD34 immunostaining (HT, hypertrophic zone; VI, vascular invasion zone). Histomorphometric quantification of boxed area is shown on the right. (**B**) Enlargement of vessels in Ranvier's groove (arrows) in $Nf1^{Prx1}$ mice. (**C**) Ingrowth of blood vessel into growth plate between hypertrophic and resting zone (transverse sections). Scale bars in (B) and (C): 100 μm and 200 μm respectively.

interferes with joint formation by the induction of a cartilage phenotype in interzone cells.

Inactivation of Nf1 results in bowing of long bones

Long bone osteopathy occurs in ~5% of NF1 patients usually presenting as unilateral anterolateral bowing of the tibia. Pathological fractures of the affected bone are frequent, and as a complication (i.e. non-union), a pseudarthrosis or 'false joint' can develop (2,23). The pathogenesis of this severe complication remains largely obscure, but analysis of the adjacent tissue has shown that inactivation of both NF1 alleles is frequent in tibial pseudarthrosis (5). Primary histological findings of resected tissue include the presence of highly cellular, little vascularized, fibromatous-like tissue, commonly associated with a thickened periosteum (24) and, in some cases, abnormal vasculature with thickened vessel walls. (25). Congenital pseudarthrosis of the tibia occurs also in the absence of the classic NF1 phenotype (23). Owing to the high similarity of the clinical and histological presentation, namely the growth of an abnormal fibrous tissue, this has been interpreted as a localized skeletal expression of NF1 in individuals with unknown/cryptic NF1 (24). Inactivation of Nf1 in mice recapitulates the human phenotype. Like in humans, bowing is already present at birth. Fractures do not occur in mice but this is most likely due to insufficient mechanical stress. The inability of mutant mice to bend their hips has to be taken into consideration because disuse leads to bone loss. Studies using either tail suspension, sciatectomy or limb immobilization to induce mechanical unloading showed a decrease in cancellous bone density and cortical thinning due to reduced osteoblast proliferation and increased bone resorption (26,27). This is in contrast to our finding that in $Nf1^{Prx1}$ mutants the osteoblast number at the cortical surface and the osteoblast proliferation *in vitro* are increased, suggesting different pathogenetic mechanisms. The reason for bowing can be found in the abnormal structure and stability of the cortical bone. Histology and BSE imaging demonstrated a dramatically increased porosity (p) of the cortical bone. Furthermore, we evaluated the local stiffness and hardness of the bone by nanoindentation, a method to determine the micrometer level elastic and plastic response of material by making small indents (with depth typically less than 1 μm) on flat polished sections (16). Nanoindentation showed a reduction in the elastic modulus (E) of the bone material itself. The average Young's modulus (relevant for the bending stiffness of the bone), which is typically given by $E(1-p)^n$, decreases not only by a reduction in E, but also by an increased porosity p (28). In the most favorable case, the reduction due to porosity is linear ($n = 1$). In other cases (e.g. in random foams or cancellous bone), the dependence is even quadratic with $n=2$ (29). Thus, the observed bending of long bones may be attributed to changes in the bone material (E, from nanoindentation) and an additional reduction inferred from the extra porosity p in the bone cortex. Staining for CD34 revealed that increased numbers of vessels contribute to the porosity of the cortical bone and thus the bending of the tibia. Another factor likely to contribute to the reduction of the stiffness E of the bone material is the reduced calcium content as demonstrated by BSE imaging.

To investigate the reasons for this finding, we cultured calvarial osteoblasts and found a reduced expression of ALP and a diminished capacity to mineralize extracellular matrix, a hallmark of differentiated osteoblasts. The reduced expression of other marker genes of osteoblast differentiation such as osteocalcin (Ocn) and integrin-binding sialoprotein (Ibsp) and their increased rate of proliferation indicate that these cells persist in an early stage of differentiation. In addition, we found an upregulation of osteopontin, a gene predominantly expressed in immature osteoblasts. Opn is a known inhibitor of calcification (30,31) and its overexpression is thus likely to contribute to the phenotype. These *in vitro* findings are in good agreement with the abnormalities observed in our $Nf1^{Prx1}$ mouse model, in particular the increased number of osteoblasts on the bone surface and the thickening of the osteoid. In agreement with our findings, it has been shown that haploinsufficiency of Nf1 results in a block of osteoblast differentiation, increased proliferation and the induction of osteopontin (32). However, loss of one Nf1 allele does not result in an overt bone phenotype, thus indicating the existence of compensatory mechanisms. Interestingly, treatment of osteoblasts with FGF has similar effects including an increase in proliferation, a reduction of ALP activity and Ocn expression, as well as an upregulation of Opn indicating a common regulatory pathway (33).

Thus, the observed thickening of the osteoid and the reduced calcium content is likely to be caused by a defect of osteoblast proliferation and differentiation. Together with an increase in porosity, this results in bone which is less resistant to mechanical forces. The asymmetries of muscle forces at the

lower limb (posterior versus anterior muscle mass) induce asymmetric strain, which leads to the observed bending. Similar mechanisms are likely to cause congenital tibial bowing in humans. Increasing mechanical forces associated with walking can be expected to potentiate these effects finally resulting in fracture and pseudarthrosis, a phenotype not observed in $Nf1^{Prx1}$ mice.

Nf1 controls proliferation and differentiation of growth plate chondrocytes

Children with NF1 characteristically have mild short stature (2). Longitudinal growth in the prenatal fetal period and after birth is generated in the growth plates through endochondral ossification, a process involving the production of cartilaginous matrix which is subsequently removed and replaced by bone (8). In $Nf1^{Prx1}$ limbs, we observed a reduced proliferation rate of the growth plate chondrocytes as well as reduction in the size of the hypertrophic zone. Ihh has been shown to be a major regulator of chondrocyte hypertrophy and proliferation through Pthrp-dependent and independent pathways (34,35). Low levels of Ihh, as observed in $Nf1^{Prx1}$ growth plates, result in reduced proliferation and a smaller zone of hypertrophy. Reduced proliferation rates, a downregulation of Ihh expression and short bones are also observed in mice carrying an activating mutation in Fgfr3 (36). Furthermore, mitogen-activated protein kinase (MAPK) pathway activation downstream of Ras signaling in chondrocytes results in an achondroplasia-like dwarfism (37), similar to phenotype observed upon Sox9 overexpression (38). Both effects, the activation of Sox9 and the downregulation of Ihh, were observed in $Nf1^{Prx1}$ growth plates, explaining, at least in part, the $Nf1^{Prx1}$ associated phenotype. Our results suggest that the short stature frequently observed in NF1 patients is caused by abnormal proliferation and differentiation of growth plate chondrocytes.

In situ expression analysis and quantitative PCR showed a strong upregulation of osteopontin (Opn), a secreted cytokine and cell attachment protein that is produced by many cell types. In bone, it is predominantly expressed in osteoblasts and in terminally differentiated chondrocytes at the chondro-osseous border (39). Opn contains an RGDS sequence motif that can promote attachment, survival and migration of several cell types, including osteoclasts and endothelial cells (40). Furthermore, Opn was shown to have an angiogenic effect in chick embryo chorioallantoic membrane (CAM) assay (41) and is known to facilitate angiogenesis in bone (42). On the basis of these findings, the overexpression of Opn is likely to contribute to the increase in osteoclasts and vasculature observed at the chondro-osseous junction of Nf1 mutant mice. Opn expression in chondrocytes and osteoblasts was shown to be induced by Fgfr3 activating mutations *in vivo* (43). In a parallel study, constitutive Fgfr3 activation resulted in increased vascular invasion and osteoclastogenesis at the chondro-osseous junction (44). Opn has been shown to be regulated by Ras. The Opn promotor contains Lef1-, Ets- and AP1-binding motifs, each of which mediates only a weak effect on transcription. However, coexpression of Pea3 and Lef1 strongly enhanced Opn promoter responsiveness (45). We found both Pea3 and Lef1 expression upregulated in $Nf1^{Prx1}$ limbs, suggesting that these transcription factors mediated the effect of increased Ras signaling on Opn.

Nf1 is involved in the regulation of vessel formation

$Nf1^{Prx1}$ mice show several abnormalities of vessel formation in the developing bone and cartilage. Cartilage is normally devoid of vessels. Supply of nutrients is accomplished by a dense layer of vessels at the chondro-osseous junction as well as by a vascular plexus surrounding the growth plate at the groove of Ranvier. We observed an increased penetration of vessels into the growth plate at the chondro-osseous junction and in the groove of Ranvier, as well as an increase in the number of vessels in the cortical bone. Using the mouse cornea neovascularization model, Wu *et al*. (46) were able to show a greater endothelial cell proliferation and an increased infiltration of inflammatory cells in $Nf1^{+/-}$ mice. An enhanced sensitivity to angiogenic factors, as recently shown for human and murine Nf1-deficient endothelial cells, is likely to underlie this phenomenon (47). A role for Ras-signaling during development of vessels is further supported by the recent finding that mutations in RASA1 cause a human venous malformation syndrome (48). As we observed a significant inactivation of Nf1 in CD31-positive endothelial cells from $Nf1^{Prx1}$ mice, the pathomechanism of vascular abnormalities is likely to have the same basis. Further studies will be needed to identify and characterize the involved pathways, but an important role of Nf1 and Ras in the development of vessels has become apparent.

In summary, our results document an important role of Nf1 in several aspects of skeletal development. Many of the observed features overlap with those found in FGF activation, thus linking the pathways. Our results indicate that NF1 associated skeletal abnormalities are caused by a primary defect in osteoblasts and/or chondrocyte differentiation due to inactivation of the NF1 gene.

MATERIALS AND METHODS

Mouse breeding and genotyping

We genotyped NF1flox and Rosa26-LacZ mice using a PCR approach as described previously (11). See Supplementary Material for primers used for detection of the Cre transgene in Prx1-Cre mouse line. All experimental procedures were approved by the 'Landesamt für Gesundheitsschutz und Technische Sicherheit (LaGeTSi), Berlin, Germany.

Protein and mRNA analysis

Whole cell lysates of passage 2 primary articular chondrocytes and calvarial osteoblasts were resolved by electrophoresis in SDS–polyacrylamide gels and transferred onto PVDF (Amersham). For western blot analysis, membranes were probed with the antibodies: phospho-p42/44 (pERK1/2) #9102 (Cell Signaling), p44 (ERK1) #4372 (Cell Signaling), p42 (ERK2) #9108 (Cell Signaling), p21/Waf1 sc-6246 (Santa Cruz), Sox9 sc-20095 (Santa Cruz), Osteopontin ($MPIIIB10_1$; DSHB) and Actin A5060 (Sigma). The Ras Activation Assay Kit (Upstate) was used according to manu-

facturer's guidelines in wild-type or $Nf1^{Prx1}$ mouse derived chondrocytes. RNA was isolated from trypsinized cells using Total RNA isolation Kit (AABiot Gdynia, Poland). Reverse transcription was performed with SuperscriptII (Invitrogen) according to manufacturer's guidelines. Gene expression was assessed by amplification of the gene of interest with Gapdh as endogenous control on a Taqman 7500 (ABI) by the SYBR green method. Primer sequences are available as Supplementary Material.

Histology, histomorphometry and *in situ* hybridization

For the histological analysis, embryos were fixed with 4% paraformaldehyde and embedded in paraffin. For histology and histomorphometry, bones were processed as previously described (49). TRAP histochemistry was performed on 5 μm sections of paraffin-embedded tibiae. The reaction occurred at 37°C in 40 mM acetate buffer pH 5.0 containing 10 mM sodium tartrate using 10 mg/ml naphthol-AS-MX-phosphate (Sigma) and 600 mg/l fast-red-violet LB-salt (Sigma) as substrate. Sections were counterstained in 0.5% light green SF yellowish (Sigma). Quantitative analysis of TRAP-positive regions was performed with the image analysis software Axiovision (Zeiss, Jena, Germany) (50). *In situ* hybridization on frozen sections of E13.5 and E14.5 embryos was performed with digoxygenin-labeled rRNA probe as described (19).

For *in vivo* BrdU labeling, newborn pups were injected with 100 μg/kg bromodeoxyuridine (Sigma) and sacrificed 8 h later.

Immunohistological stainings

7 μm paraffin sections were subjected to pH 6.0 citrate buffer/microwave antigen retrieval. Staining was performed with anti-BrdU #1-299-964 antibody (Roche) 1:100, anti Sox9 H-90 antibodies (Santa Cruz) at 1:400 and anti CD34 Mec 14.7 (Abcam) antibody at 1:100.

Three-dimensional imaging by μCT and OPT

Bone specimens were scanned at 32 μm resolution using a prototype μCT scanner. Three-dimensional reconstruction was done by the Amira software version 3.1. (51). Alizarin red/ Alcian blue stained skeletal preparations were scanned by the OPT method, which accumulates projection images of a entire specimen from many different angles and recalculates the original three-dimensional structure by using a 'back-projection' reconstruction algorithm (52). OPT-Scans were performed with UV light in darkfield illumination using GFP1 and Texas-Red filters to detect the complete morphology and the Alizarin red staining, respectively. Another OPT-Scan in brightfield illumination detected the Alcian blue staining. Virtual sections of the original three-dimensional reconstructions can be viewed at free angles and analyzed using the free software of the Edinburgh Mouse Atlas Project (EMAP, http://genex.hgu.mrc.ac.uk/). QuickTime movies were generated in the IPLab software from ScanAnalytics.

BSE microscopy and nanoindentation

BSE images were obtained using environmental scanning electron microscope operated at accelerating voltage of 12.5 kV under low vacuum as previously described (16). The sample to detector distance was 10 mm. All the images were taken at 800× magnification in the mid-shaft region of bone. To calculate the relative porosity in the bone, two areas, each of about 75 × 175 μm from each sample were used and converted into gray scales. Nanoindentation testing was performed using a scanning nanoindenter (Hysitron Ubi1, USA) with a Berkovich diamond indenter tip as previously described (16). The indents were performed using a maximum force of 5000 μN with a hold time of 60 s at maximum force. Er, nanoindentation modulus measured (in GPa), reflects the stiffness of the material determined based on the slope of the unloading curve in the region of 20–95% of maximum load.

Primary osteoblast, osteoclast and chondrocyte culture

Primary osteoblasts were isolated from calvariae of P3 wt and $Nf1^{Prx1}$ mice by digestion with 0,1% collagenase for 2×30 min at 37°C. Cells were seeded at a density of $2\times104/cm^2$ in cell culture flasks and cultured in αMEM with 10% FCS. After reaching confluency, the cells were stimulated by adding 10 mM β-glycerolphosphate and 0.28 mM ascorbic acid to the culture medium (day 0). Cells were cultured until day 12. Quantitative ALP and mineralization assays were performed at days 4, 8 and 12 of culture as previously described (53). Briefly, ALP activity was determined by homogenizing three replicates separately in ALP-buffer1 (0.1 M glycine, 1% NP-40, 1 mM $MgCl_2$, 1 mM $ZnCl_2$). After the addition of 1 vol of ALP-buffer2 [5 mM *p*-nitrophenyl phosphate (*p*-NPP), 0.1 M glycine, pH 9.6, 1 mM $MgCl_2$ and 1 mM $ZnCl_2$], reactions were incubated at 37°C for 30 min and stopped by addition of 1 M NaOH. The amount of *p*-NP released from the substrate *p*-NPP was recorded at 405 nm. ALP activity is given as unit of absorption/μg protein/30 min.

Parallel to the ALP assay, mineralization was monitored by Alizarin red staining. Osteoclast precursors were isolated from bone marrow and cultured as described by Takeshita *et al*. (54). Chondrocytes were isolated from hyaline cartilage of P4 knee and elbow joints using previously described methods (55). Briefly, cartilage was dissected free of fibrous tissue and bone, and stored overnight at 4°C in DMEM medium before proceeding with the collagenase digestion. In order to minimize non-cartilaginous cell contamination, two steps of digests were done, each at 37°C for 1 h, and only cells from second one were harvested. Second passage cells were used in all experiments.

FACS sorting of endothelial cells

Lung tissue was minced and digested in 0.1% collagenase/PBS for 1 h at 37°C. Long bones were minced and washed in PBS. Cell suspensions were incubated with an FITC-labeled anti-CD31 antibody (BD Pharmingen), washed and cell sorting was performed according to standard procedures.

Statistical analysis

Analysis of histomorphometric results was performed using $n = 5$ animals and 20 sections per group. All values were expressed as the mean $\pm$ SD. The statistical difference between the two groups was examined using Student's unpaired t-test. $^{*}P < 0.05$; $^{**}P < 0.01$.

SUPPLEMENTARY MATERIAL

Supplementary Material is available at HMG Online.

ACKNOWLEDGEMENTS

R.S. and B.H. would like to thank James Sharpe, Harris Morrison and Tim Mohun for their help with setting up the OPT equipment. We thank M. Giehl and D. Felsenberg for microCT scanning. The antibody MPIIIB10$_1$ developed by M. Solursh was obtained from the Developmental Studies Hybridoma Bank. We thank Victor Mautner, Universitätsklinikum Hamburg, Germany, for providing us with an X-ray showing tibial bowing (Fig. 2B) in an NF1 patient. We acknowledge Monika Osswald and Kathrin Seidel for excellent technical assistance. S.M., M.K. and J.K. were supported by grants from the Deutsche Forschungsgemeinschaft and the US-Army grant DAMD17-03-1-0183.

Conflict of Interest statement. None declared.

REFERENCES

1. Riccardi, V.M. (1999) InFriedman, J.M., Gutmann, D.H., MacCollin, M. and Riccardi, V.M. (eds), *Neurofibromatosis: Phenotype, Natural History, and Pathogenesis*. John Hopkins Press, Baltimore, pp. 1–25.
2. Alwan, S., Tredwell, S.J. and Friedman, J.M. (2005) Is osseous dysplasia a primary feature of neurofibromatosis 1 (NF1)? *Clin. Genet.*, **67**, 378–390.
3. Stevenson, D.A., Birch, P.H., Friedman, J.M., Viskochil, D.H., Balestrazzi, P., Boni, S., Buske, A., Korf, B.R., Niimura, M., Pivnick, E.K. *et al*. (1999) Descriptive analysis of tibial pseudarthrosis in patients with neurofibromatosis 1. *Am. J. Med. Genet.*, **84**, 413–419.
4. Ruggieri, M., Pavone, V., De Luca, D., Franzo, A., Tine, A. and Pavone, L. (1999) Congenital bone malformations in patients with neurofibromatosis type 1 (Nf1). *J. Pediatr. Orthop.*, **19**, 301–305.
5. Stevenson, D.A., Zhou, H., Ashrafi, S., Messiaen, L.M., Carey, J.C., D'Astous, J.L., Santora, S.D. and Viskochil, D.H. (2006) Double Inactivation of NF1 in tibial pseudarthrosis. *Am. J. Hum. Genet.*, **79**, 143–148.
6. Martin, G.A., Viskochil, D., Bollag, G., McCabe, P.C., Crosier, W.J., Haubruck, H., Conroy, L., Clark, R., O'Connell, P., Cawthon, R.M. *et al*. (1990) The GAP-related domain of the neurofibromatosis type 1 gene product interacts with ras p21. *Cell*, **63**, 843–849.
7. Frame, S. and Balmain, A. (2000) Integration of positive and negative growth signals during ras pathway activation *in vivo*. *Curr. Opin. Genet. Dev.*, **10**, 106–113.
8. Kornak, U. and Mundlos, S. (2003) Genetic disorders of the skeleton: a developmental approach. *Am. J. Hum. Genet.*, **73**, 447–474.
9. Tartaglia, M., Mehler, E.L., Goldberg, R., Zampino, G., Brunner, H.G., Kremer, H., van der Burgt, I., Crosby, A.H., Ion, A., Jeffery, S. *et al*. 6(2001) Mutations in PTPN11, encoding the protein tyrosine phosphatase SHP-2, cause Noonan syndrome. *Nat. Genet.*, **29**, 465–468.
10. Schubbert, S., Zenker, M., Rowe, S.L., Boll, S., Klein, C., Bollag, G., van der Burgt, I., Musante, L., Kalscheuer, V., Wehner, L.E. *et al*. (2006) Germline KRAS mutations cause Noonan syndrome. *Nat. Genet.*, **38**, 331–336.
11. Zhu, Y., Romero, M.I., Ghosh, P., Ye, Z., Charnay, P., Rushing, E.J., Marth, J.D. and Parada, L.F. (2001) Ablation of NF1 function in neurons induces abnormal development of cerebral cortex and reactive gliosis in the brain. *Genes Dev.*, **15**, 859–876.
12. Vogel, K.S., Klesse, L.J., Velasco-Miguel, S., Meyers, K., Rushing, E.J. and Parada, L.F. (1999) Mouse tumor model for neurofibromatosis type 1. *Science*, **286**, 2176–2179.
13. Dasgupta, B. and Gutmann, D.H. (2003) Neurofibromatosis 1: closing the GAP between mice and men. *Curr. Opin. Genet. Dev.*, **13**, 20–27.
14. Logan, M., Martin, J.F., Nagy, A., Lobe, C., Olson, E.N. and Tabin, C.J. (2002) Expression of Cre recombinase in the developing mouse limb bud driven by a Prxl enhancer. *Genesis*, **33**, 77–80.
15. Akiyama, H., Chaboissier, M.C., Martin, J.F., Schedl, A. and de Crombrugghe, B. (2002) The transcription factor Sox9 has essential roles in successive steps of the chondrocyte differentiation pathway and is required for expression of Sox5 and Sox6. *Genes Dev.*, **16**, 2813–2828.
16. Gupta, H.S., Schratter, S., Tesch, W., Roschger, P., Berzlanovich, A., Schoeberl, T., Klaushofer, K. and Fratzl, P. (2005) Two different correlations between nanoindentation modulus and mineral content in the bone-cartilage interface. *J. Struct. Biol.*, **149**, 138–148.
17. Shapiro, F., Holtrop, M.E. and Glimcher, M.J. (1977) Organization and cellular biology of the perichondrial ossification groove of ranvier: a morphological study in rabbits. *J. Bone Joint Surg. Am.*, **59**, 703–723.
18. Pacifici, M., Koyama, E. and Iwamoto, M. (2005) Mechanisms of synovial joint and articular cartilage formation: recent advances, but many lingering mysteries. *Birth Defects Res. C Embryo Today*, **75**, 237–248.
19. Seemann, P., Schwappacher, R., Kjaer, K.W., Krakow, D., Lehmann, K., Dawson, K., Stricker, S., Pohl, J., Ploger, F., Staub, E. *et al*. (2005) Activating and deactivating mutations in the receptor interaction site of GDF5 cause symphalangism or brachydactyly type A2. *J. Clin. Invest.*, **115**, 2373–2381.
20. Storm, E.E. and Kingsley, D.M. (1999) GDF5 coordinates bone and joint formation during digit development. *Dev. Biol.*, **209**, 11–27.
21. Bell, D.M., Leung, K.K., Wheatley, S.C., Ng, L.J., Zhou, S., Ling, K.W., Sham, M.H., Koopman, P., Tam, P.P. and Cheah, K.S. (1997) SOX9 directly regulates the type-II collagen gene. *Nat. Genet.*, **16**, 174–178.
22. Wang, Q., Green, R.P., Zhao, G. and Ornitz, D.M. (2001) Differential regulation of endochondral bone growth and joint development by FGFR1 and FGFR3 tyrosine kinase domains. *Development*, **128**, 3867–3876.
23. Hefti, F., Bollini, G., Dungl, P., Fixsen, J., Grill, F., Ippolito, E., Romanus, B., Tudisco, C. and Wientroub, S. (2000) Congenital pseudarthrosis of the tibia: history, etiology, classification, and epidemiologic data. *J. Pediatr. Orthop. B*, **9**, 11–15.
24. Ippolito, E., Corsi, A., Grill, F., Wientroub, S. and Bianco, P. (2000) Pathology of bone lesions associated with congenital pseudarthrosis of the leg. *J. Pediatr. Orthop. B*, **9**, 3–10.
25. Kuorilehto, T., Kinnunen, P., Nissinen, M., Alanne, M., Leskelä, H.-V., Lehenkari, P. and Peltonem, J. Vasculopathy in two cases of NF1-related congenital pseudoarthrosis. *Pathol. Res. Pract.*, **202**, 687–690.
26. Barou, O., Palle, S., Vico, L., Alexandre, C. and Lafage-Proust, M.H. (1998) Hindlimb unloading in rat decreases preosteoblast proliferation assessed *in vivo* with BrdU incorporation. *Am. J. Physiol.*, **274**, E108–E114.
27. Machwate, M., Zerath, E., Holy, X., Pastoureau, P. and Marie, P.J. (1994) Insulin-like growth factor-I increases trabecular bone formation and osteoblastic cell proliferation in unloaded rats. *Endocrinology*, **134**, 1031–1038.
28. Greenleaf, J.F., Fatemi, M. and Insana, M. (2003) Selected methods for imaging elastic properties of biological tissues. *Annu. Rev. Biomed. Eng.*, **5**, 57–78.
29. Gibson, L.J. and Asby, M.F. (2001) InGibson, L.J. and Ashby, M.F. (eds), *Cellular Solids, Structure and Properties*, Cambridge University Press—Edinburgh Building, Cambridge CB2 2RU, UK; 40 West 20th Street, New York, NY 1011-4211, USA; 10 Stanford Road, Oakleigh, Melbourne 3166, Australia.
30. Boskey, A.L., Spevak, L., Paschalis, E., Doty, S.B. and McKee, M.D. (2002) Osteopontin deficiency increases mineral content and mineral crystallinity in mouse bone. *Calcif. Tissue Int.*, **71**, 145–154.
31. Pampena, D.A., Robertson, K.A., Litvinova, O., Lajoie, G., Goldberg, H.A. and Hunter, G.K. (2004) Inhibition of hydroxyapatite formation by osteopontin phosphopeptides. *Biochem. J.*, **378**, 1083–1087.
32. Yu, X., Chen, S., Potter, O.L., Murthy, S.M., Li, J., Pulcini, J.M., Ohashi, N., Winata, T., Everett, E.T., Ingram, D. *et al*. (2005) Neurofibromin and its inactivation of Ras are prerequisites for osteoblast functioning. *Bone*, **36**, 793–802.

33. Tang, K.T., Capparelli, C., Stein, J.L., Stein, G.S., Lian, J.B., Huber, A.C., Braverman, L.E. and DeVito, W.J. (1996) Acidic fibroblast growth factor inhibits osteoblast differentiation *in vitro*: altered expression of collagenase, cell growth-related, and mineralization-associated genes. *J. Cell. Biochem.*, **61**, 152–166.
34. Kobayashi, T., Soegiarto, D.W., Yang, Y., Lanske, B., Schipani, E., McMahon, A.P. and Kronenberg, H.M. (2005) Indian hedgehog stimulates periarticular chondrocyte differentiation to regulate growth plate length independently of PTHrP. *J. Clin. Invest.*, **115**, 1734–1742.
35. Minina, E., Kreschel, C., Naski, M.C., Ornitz, D.M. and Vortkamp, A. (2002) Interaction of FGF, Ihh/Pthlh, and BMP signaling integrates chondrocyte proliferation and hypertrophic differentiation. *Dev. Cell*, **3**, 439–449.
36. Chen, L., Li, C., Qiao, W., Xu, X. and Deng, C. (2001) A Ser(365) → Cys mutation of fibroblast growth factor receptor 3 in mouse downregulates Ihh/PTHrP signals and causes severe achondroplasia. *Hum. Mol. Genet.*, **10**, 457–465.
37. Murakami, S., Kan, M., McKeehan, W.L. and de Crombrugghe, B. (2000) Up-regulation of the chondrogenic Sox9 gene by fibroblast growth factors is mediated by the mitogen-activated protein kinase pathway. *Proc. Natl Acad. Sci USA*, **97**, 1113–1118.
38. Akiyama, H., Lyons, J.P., Mori-Akiyama, Y., Yang, X., Zhang, R., Zhang, Z., Deng, J.M., Taketo, M.M., Nakamura, T., Behringer, R.R. *et al*. (2004) Interactions between Sox9 and beta-catenin control chondrocyte differentiation. *Genes Dev.*, **18**, 1072–1087.
39. Denhardt, D.T., Noda, M., O'Regan, A.W., Pavlin, D. and Berman, J.S. (2001) Osteopontin as a means to cope with environmental insults: regulation of inflammation, tissue remodeling, and cell survival. *J. Clin. Invest.*, **107**, 1055–1061.
40. Standal, T., Borset, M. and Sundan, A. (2004) Role of osteopontin in adhesion, migration, cell survival and bone remodeling. *Exp Oncol.*, **26**, 179–184.
41. Leali, D., Dell'Era, P., Stabile, H., Sennino, B., Chambers, A.F., Naldini, A., Sozzani, S., Nico, B., Ribatti, D. and Presta, M. (2003) Osteopontin (Eta-1) and fibroblast growth factor-2 cross-talk in angiogenesis. *J. Immunol.*, **171**, 1085–1093.
42. Asou, Y., Rittling, S.R., Yoshitake, H., Tsuji, K., Shinomiya, K., Nifuji, A., Denhardt, D.T. and Noda, M. (2001) Osteopontin facilitates angiogenesis, accumulation of osteoclasts, and resorption in ectopic bone. *Endocrinology*, **142**, 1325–1332.
43. Chen, L., Adar, R., Yang, X., Monsonego, E.O., Li, C., Hauschka, P.V., Yayon, A. and Deng, C.X. (1999) Gly369Cys mutation in mouse FGFR3 causes achondroplasia by affecting both chondrogenesis and osteogenesis. *J. Clin. Invest.*, **104**, 1517–1525.
44. Segev, O., Chumakov, I., Nevo, Z., Givol, D., Madar-Shapiro, L., Sheinin, Y., Weinreb, M. and Yayon, A. (2000) Restrained chondrocyte proliferation and maturation with abnormal growth plate vascularization and ossification in human FGFR-3(G380R) transgenic mice. *Hum. Mol. Genet.*, **9**, 249–258.
45. El-Tanani, M., Platt-Higgins, A., Rudland, P.S. and Campbell, F.C. (2004) Ets gene PEA3 cooperates with beta-catenin-Lef-1 and c-Jun in regulation of osteopontin transcription. *J. Biol. Chem.*, **279**, 20794–20806.
46. Wu, M., Wallace, M.R. and Muir, D. (2006) Nf1 haploinsufficiency augments angiogenesis. *Oncogene*, **25**, 2297–2303.
47. Munchhof, A.M., Li, F., White, H.A., Mead, L.E., Krier, T.R., Fenoglio, A., Li, X., Yuan, J., Yang, F.C. and Ingram, D.A. (2006) Neurofibroma-associated growth factors activate a distinct signaling network to alter the function of neurofibromin-deficient endothelial cells. *Hum. Mol. Genet.*, **15**, 1858–1869.
48. Boon, L.M., Mulliken, J.B. and Vikkula, M. (2005) RASA1: variable phenotype with capillary and arteriovenous malformations. *Curr. Opin. Genet. Dev.*, **15**, 265–269.
49. Hahn, M., Vogel, M. and Delling, G. (1991) Undecalcified preparation of bone tissue: report of technical experience and development of new methods. *Virchows Arch. A Pathol. Anat. Histopathol.*, **418**, 1–7.
50. Parfitt, A.M., Drezner, M.K., Glorieux, F.H., Kanis, J.A., Malluche, H., Meunier, P.J., Ott, S.M. and Recker, R.R. (1987) Bone histomorphometry: standardization of nomenclature, symbols, and units. Report of the ASBMR Histomorphometry Nomenclature Committee. *J. Bone Miner. Res.*, **2**, 595–610.
51. Stalling, D., Westerhoff, M. and Hege, C. (2005) Amira: a highly interactive system for visual data analysis. In Hansen, C.D. and Johnson, C.R. (eds), *The Vizualization Handbook*. Elsevier—Sara Burgerhartstraat 25 1055kv Amsterdam, Chapter 38, pp. 749–767.
52. Sharpe, J., Ahlgren, U., Perry, P., Hill, B., Ross, A., Hecksher-Sorensen, J., Baldock, R. and Davidson, D. (2002) Optical projection tomography as a tool for 3D microscopy and gene expression studies. *Science*, **296**, 541–545.
53. Knaus, P. and Sebald, W. (2001) Cooperativity of binding epitopes and receptor chains in the BMP/TGFbeta superfamily. *Biol. Chem.*, **382**, 1189–1195.
54. Takeshita, S., Kaji, K. and Kudo, A. (2000) Identification and characterization of the new osteoclast progenitor with macrophage phenotypes being able to differentiate into mature osteoclasts. *J. Bone Miner. Res.*, **15**, 1477–1488.
55. Chan, D., Taylor, T.K. and Cole, W.G. (1993) Characterization of an arginine 789 to cysteine substitution in alpha 1 (II) collagen chains of a patient with spondyloepiphyseal dysplasia. *J. Biol. Chem.*, **268**, 15238–15245.